CARBON 75 (2014) 169–177

Available at www.sciencedirect.com

ScienceDirect

journal homepage: www.elsevier.com/locate/carbon

Duality of the interfacial thermal conductance in graphene-based nanocomposites

Ying Liu [a], Jingsong Huang [b], Bao Yang [c], Bobby G. Sumpter [b], Rui Qiao [a,*]

[a] Department of Mechanical Engineering, Clemson University, Clemson, SC 29634-0921, USA
[b] Center for Nanophase Materials Science and Computer Science & Mathematics Division, Oak Ridge National Laboratory, Bethel Valley Road, Oak Ridge, TN 37831-6367, USA
[c] Department of Mechanical Engineering, University of Maryland, College Park, MD 20742, USA

ARTICLE INFO

Article history:
Received 24 December 2013
Accepted 27 March 2014
Available online 4 April 2014

ABSTRACT

The thermal conductance of graphene–matrix interfaces plays a key role in controlling the thermal properties of graphene-based nanocomposites. Using atomistic simulations, we found that the interfacial thermal conductance depends strongly on the mode of heat transfer at graphene–matrix interfaces: if heat enters graphene from one side of its basal plane and immediately leaves it through the other side, the corresponding interfacial thermal conductance, G_{across}, is large; if heat enters graphene from both sides of its basal plane and leaves it at a position far away on its basal plane, the corresponding interfacial thermal conductance, $G_{non\text{-}across}$, is small. For a single-layer graphene immersed in liquid octane, G_{across} is ~150 MW/m^{2}K while $G_{non\text{-}across}$ is ~5 MW/m^{2}K. G_{across} decreases with increasing multi-layer graphene thickness (i.e., number of layers in graphene) and approaches an asymptotic value of 100 MW/m^{2}K for 7-layer graphenes. $G_{non\text{-}across}$ increases only marginally as the graphene sheet thickness increases. Such a duality of the interface thermal conductance for different probing methods and its dependence on graphene sheet thickness can be traced ultimately to the unique physical and chemical structure of graphene materials. The ramifications of these results in areas such as the optimal design of graphene-based thermal nanocomposites are discussed.

1. Introduction

Thermal nanocomposites featuring nanoscale fillers with high thermal conductivity dispersed in low-conductivity matrix materials play a key role in many high-profile thermal management applications, e.g., serving as thermal interface materials in microelectronics cooling systems [1]. Recent development of graphene-based thermal nanocomposites is triggered by the discovery that graphene has extremely high thermal conductivities ~1000–5000 W/mK at room-temperature when suspended in vacuum [2–5]. While graphene's thermal conductivity tends to decrease when it is supported on substrates or embedded into matrices [6–9], graphene-based nanocomposites displaying impressive effective thermal conductivities have been developed by several groups [10–13]. To enable rational design of graphene-based nanocomposites, so that their performance in terms of effective thermal conductivities can be further improved, a fundamental understanding of the thermal transport in such materials is essential.

* *Corresponding author.*
E-mail address: rqiao@clemson.edu (R. Qiao).
http://dx.doi.org/10.1016/j.carbon.2014.03.050

Extensive research has concluded that the interfacial thermal conductance between nanoscale fillers and matrix materials plays a central role in determining the effective thermal conductivity of nanocomposites [9,14–20]. The thermal conductance at the interfaces between graphene and various materials has been measured using different experimental techniques in recent years, giving values ranging from 10 to 200 MW/m^{2}K [2,3,21–24]. The difference in the measured conductance is typically attributed to the difference in how graphene and matrix materials were prepared in those experiments. The thermal conductance at the interfaces between graphene and soft materials such as organic liquids and polymeric melts has also been computed using molecular dynamics (MD) simulations [25–29]. Depending on the method used to compute thermal conductance, different values have been obtained. For example, the thermal relaxation method, in which the evolution of graphene's temperature was monitored after heat was injected into it, yielded relatively low thermal conductance (e.g., ~10–20 MW/m^{2}K) [27]. It was recently clarified that the thermal conductance probed in such a way is more relevant to the situation found in a pump–probe experimental setup [25]. The more common method, in which heat is simultaneously injected into and removed from different portions of the matrix materials to create heat flux through a graphene surface, probes thermal conductance that is more relevant to that measured in thermal nanocomposites. Calculations based on such a method usually yield relatively high thermal conductance, e.g., ~30–200 MW/m^{2}K for graphene–polymer interfaces.[25,26,28] The physical origins of the different thermal conductance in such a wide range are not fully understood.

In this work, we use MD simulations to examine the thermal conductance at graphene–matrix interfaces through two different heat transfer modes. We show that, depending on the mode of heat transfer at these interfaces, the thermal conductance at the same graphene–matrix interface can differ by nearly two orders of magnitude and it also exhibits distinct dependence on the graphene layer thickness. We trace these different behaviors ultimately to the unique physical and chemical structure of graphene materials. These results have rich ramifications in areas such as experimental characterization of thermal conductivity of graphene and the design of graphene-based thermal nanocomposites.

2. Simulations and Methods

We examine the heat conduction at graphene–matrix interfaces using non-equilibrium MD (NEMD) simulations. To model the graphene-based thermal nanocomposite systems studied in various experiments, single-layer and AB-stacked multi-layer graphene sheets are used as the nanoscale fillers. Liquid octane, in which the nature of heat conduction is similar to that in a broad range of soft materials such as oil, grease, and polymer melts, is adopted as the matrix material.

2.1. NEMD simulations

Two types of model systems are used in the simulations. The first system, as shown in Fig. 1a, features a graphene sheet with one through seven graphene layers, with a lateral dimension of 6.01×6.76 nm^2 spanning the entire simulation box with 6.00 nm thick liquid octane on the upper and lower sides. To simulate the thermal transport in nanocomposites, a constant heat flux q'' is imposed across the system by injecting (removing) heat into (from) the octane molecules in the region that is 4.00–5.00 nm above (below) the graphene surface [25]. To determine the interfacial conductance, the temperature profile of octane in the direction normal to the graphene surface, $T_{oct}(z)$, is computed. By extrapolating $T_{oct}(z)$ into the space occupied by the graphene layer, the temperature drop in this space, ΔT_{oct}, is retrieved. When the graphene sheet consists of more than one graphene layer, the temperature drop within the graphene sheet, ΔT_{gn}, is also retrieved. The interfacial conductance is computed using $G = 2q''/(\Delta T_{oct} - \Delta T_{gn})$, where the factor of 2 accounts for the existence of two graphene–octane interfaces in the system. This method has been used extensively for computing the interfacial thermal conductance at various interfaces [28,30,31]. A key feature of this system is that heat enters the graphene sheet from one side of its basal plane and immediately leaves through the other side, i.e., heat directly passes across the graphene sheet. In nanocomposites, this mode of interfacial thermal transport is encountered only when graphene sheets are perfectly aligned and the overall heat flux through the composite is in the direction normal to graphene's basal plane.

In typical nanocomposites, the overall heat flux is rarely in the direction normal to graphene sheets and the dominant mode of interfacial heat conduction is that heat enters graphene at one position on its basal plane and leaves at a position away on its basal plane, thus involving heat conduction within the graphene sheet in the in-plane direction. To study this mode of interfacial thermal transport, a second system shown in Fig. 1b is used. Here, the graphene sheet is placed in the middle of the simulation box and heat flux across the system is imposed using the heat injection/removal scheme shown in Fig. 1b. The lengths of the graphene sheet and simulation box are 86.44 and 110.2 nm, respectively. The thickness of the octane layer h_o is 1.3–1.45 nm in depending on the thickness of the graphene sheet in the system. Because of the high computational cost due to the large system size, here we only considered graphene sheets with one through three graphene layers, and the width of the system in the y-direction is chosen as 2.60 nm. During simulations, the average temperature profiles of octane and graphene in the x-direction, $T_{oct}(x)$ and $T_{gn}(x)$, are recorded. To extract the interfacial conductance in this system, the usual method is to fit the effective conductivity of the simulated system to the prediction by effective medium theory using interfacial conductance as an adjustable parameter. This method requires the conductivity of the graphene *embedded inside the matrix* as an input, which is unknown *a priori* and sometimes assumed to be the same as that of graphene suspended in vacuum. Here, we use two different methods.

In the first method, we model the system shown in Fig. 1b using the classical heat conduction equation, which is solved by the finite element method (FEM). The thermal conductivity k_o of both bulk and confined liquid octane is calculated from separate NEMD simulations. The thermal conductivity of graphene and the interfacial conductance in the heat

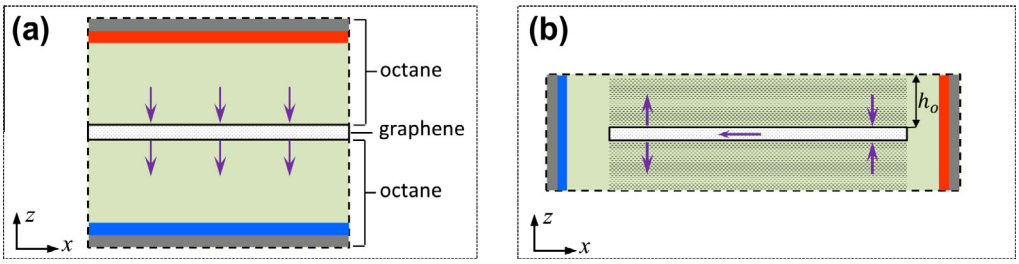

Fig. 1 – Schematic of the two types of MD systems for studying heat conduction at graphene–octane interfaces: (a) heat enters graphene from one side of its basal plane and immediately leaves through the other side. The corresponding interfacial thermal conductance is termed as G_{across}; (b) heat enters graphene from both sides of its basal plane and leaves the graphene at a position far away. The corresponding interfacial thermal conductance is termed as $G_{non\text{-}across}$. Red (blue) region denotes the heat source (sink) zone; gray regions (thickness = 1.00 nm) denote the space in which octane molecules are frozen to avoid thermal short-circuiting. The purple arrows denote heat fluxes. The dashed lines denote the periodic simulation box. (A colour version of this figure can be viewed online.)

conduction equation are tuned until $T_{oct}(x)$ and $T_{gn}(x)$ predicted by the FEM model match those by the MD simulations. This method assumes that the classical heat conduction equation is valid for graphene embedded in a matrix. To eliminate this assumption, we adopt a second method. Using the diagram shown in Fig. 2b, one can show that the temperature of octane inside the space above and beneath the graphene sheet (shaded region in Figs. 1 and 2b) is governed by

$$\frac{\partial^2}{\partial x^2} T_{oct}(x) = \frac{G}{k_o h_o} [T_{oct}(x) - T_{gn}(x)], \quad (1)$$

where k_o is the thermal conductivity (in units of W/mK), h_o the thickness of the octane layer above/beneath the graphene (in units of m), and G the interfacial thermal conductance (in units of W/m^2K). In deriving Eq. (1), the temperature of the octane layer above/beneath graphene is assumed to be uniform in the z-direction. Therefore, Eq. (1) is valid only in the region where the temperature variation within octane (along the z-direction) is much smaller than the temperature difference between octane and graphene. To calculate the interfacial conductance, by defining $\Delta T_{oct\text{-}gn} = |T_{oct} - T_{gn}|$ for

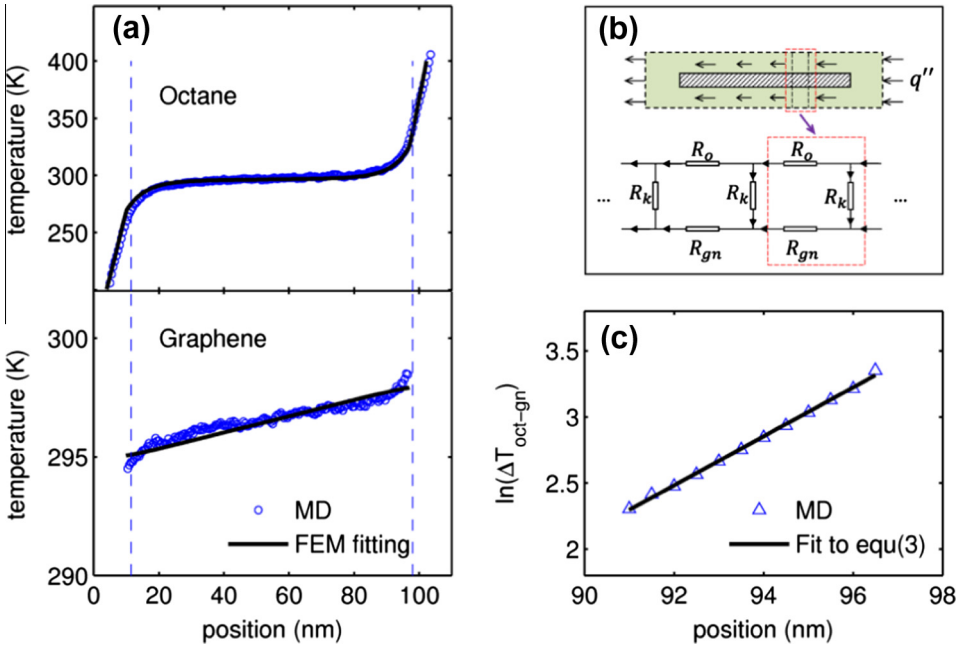

Fig. 2 – Calculation of interfacial thermal conductance G in systems shown in Fig. 1b: (a) Fitting of the graphene (lower panel) and octane (upper panel) temperature profiles predicted by FEM model to MD results using the thermal conductivity of graphene and G as adjustable parameters. (b) Circuit model for deriving the governing equation (Eq. (1)) for the temperature profile of the octane layer in the shaded region in Fig. 1b. $R_o = h_o/k_o$ is the thermal resistance of the octane layer surrounding the graphene sheet, $R_k = 1/G$ is the thermal resistance of the graphene–octane interface, and R_{gn} is the thermal resistance of the graphene sheet. (c) Fitting of ln ($\Delta T_{oct\text{-}gn}$) in region near the right end of the graphene sheet embedded in liquid octane (cf. Fig. 1b). In (a) and (c), the graphene sheet is a single-layer graphene of 86.44 nm in length. (A colour version of this figure can be viewed online.)

the region near the two ends of the graphene sheet where the gradient of $T_{gn}(x)$ is much smaller than that of $T_{oct}(x)$, Eq. (1) becomes

$$\frac{\partial^2}{\partial x^2}\Delta T_{oct-gn} = \frac{\Delta T_{oct-gn}}{k_o h_o / G} \tag{2}$$

Using the general solution of Eq. (2), i.e., $\Delta T_{oct-gn} = a \cdot \exp(x/\sqrt{k_o h_o / G})$, we obtain

$$\ln(\Delta T_{oct-gn}) = x/\sqrt{k_o h_o / G} + \ln a \tag{3}$$

where a is a constant. Therefore, by fitting $\ln(\Delta T_{oct\text{-}gn})$ to a linear function $f(x) = sx + b$, G can be determined as

$$G = k_o h_o s^2 \tag{4}$$

The mode of interfacial heat conduction probed in the system shown in Fig. 1b differs qualitatively from that probed in the system shown in Fig. 1a, and as to be shown later, the interfacial conductance inferred from these systems also differs greatly. To facilitate discussions, the interfacial conductance computed from the system in Fig. 1a, in which heat passes *across* the graphene sheet, is denoted as G_{across}, while the interfacial conductance computed from the system in Fig. 1b is denoted as $G_{non\text{-}across}$.

2.2. MD details

Graphene is modeled using the force fields developed in Ref. [32], which can be used to accurately reproduce the thermal and mechanical properties of graphene such as thermal conductivity. Octane molecules are modeled using united atom force fields [33]. The number of octane molecules inside each system is adjusted so that the octane density is 0.69 g/cc at a position away from the graphene sheet. All simulations are performed using the LAMMPS package [30]. Each system is equilibrated in the NVT ensemble (T = 300 K) for 2 ns and followed by a further equilibration of 3 ns in the NVE ensemble. Using the schemes shown in Fig. 1, constant heat flux is imposed at the end of equilibration and the system is evolved in the NVE ensemble for 50 ns using a time step of 0.5 fs. The temperature distributions of the graphene and the octane matrix retrieved during the last 20 ns of the trajectory are used for computing G_{across} and $G_{non\text{-}across}$. Each system is simulated with three different initial configurations and two different heat fluxes.

3. Results and discussion

Using the methods described above, we investigated the thermal transport at the graphene–octane interfaces in the two types of systems shown in Fig. 1. Since thermal transport in the first type of system (cf. Fig. 1a) has been studied extensively and our simulations show similar features as revealed in prior studies [26], interfacial thermal conductance results are given below without presenting further details for brevity. For the second type of system (cf. Fig. 1b), Fig. 2a shows the temperature profiles of octane and graphene sheet, $T_{oct}(x)$ and $T_{gn}(x)$, in the case of a single-layer graphene. As expected, near the right end of graphene, $T_{oct}(x)$ is higher than $T_{gn}(x)$, indicating that heat enters from octane into graphene, and the opposite process occurs near the left end of graphene. The mode of heat transfer at these graphene–octane interfaces is thus consistent with that depicted in Fig. 1b. With the thermal conductivity of the liquid octane plugged in, $T_{oct}(x)$ and $T_{gn}(x)$ predicted by the FEM model can match those obtained in the MD simulations when the thermal conductivity of graphene and the conductance of graphene–octane interface $G_{non\text{-}across}$ are tuned to 340 W/m·K and 4.97 MW/m^{2}K, respectively. We also determine $G_{non\text{-}across}$ using $T_{oct}(x)$ and $T_{gn}(x)$ based on Eq. (4). Specifically, we fit the difference between the average octane temperature and the graphene temperature, $\ln(\Delta T_{oct\text{-}gn})$, as a linear function of the x-position in the region near the right end of the graphene sheet (from x = 91.0–96.5 nm, see Fig. 2c). In this region, the variation of octane's temperature in the z-direction is much smaller than the temperature difference between octane liquids and the graphene (e.g., at x = 94 nm, the octane temperature varies from 315.2 to 317.1 K in the z-direction but the local temperature of graphene is 297.8 K), hence Eq. (1) is valid. Fig. 2a and c show that, in the region where we performed fitting, the variation of $T_{oct}(x)$ in the x-direction is far greater than that of $T_{gn}(x)$ and $\ln(\Delta T_{oct\text{-}gn})$ can be fit to a linear function. Therefore, it is safe to extract $G_{non\text{-}across}$ using the second method (see Section 2.1). Similar fitting is obtained near the left end of the graphene sheet, giving very similar results (not shown). $G_{non\text{-}across}$ computed from such linear regressions based on Eq. (4) is 4.32 ± 0.44 MW/m^{2}K, in good agreement with that computed using the first method. By comparing $G_{non\text{-}across}$ extracted from this method to that from the first method, we expect the uncertainty of extracted $G_{non\text{-}across}$ to be less than 15% using the second method.

Fig. 3 summarizes the thermal conductance of graphene–octane interfaces corresponding to the two different modes of interfacial thermal transport. The interfacial conductance corresponding to the thermal transport mode shown in Fig. 1a, G_{across}, is very large at ~150 MW/m^{2}K for single-layer graphene; it decreases as the thickness of graphene sheet increases, reaching an asymptotic value of ~100 MW/m^{2}K for 7-layer graphenes. The interfacial conductance corresponding to the thermal transport mode shown in

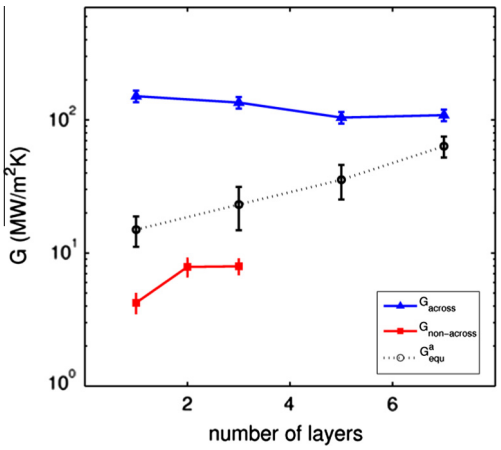

Fig. 3 – Interfacial thermal conductance at graphene–octane interfaces probed using various methods for the systems shown in Fig. 1. (A colour version of this figure can be viewed online.)

Fig. 1b, $G_{non\text{-}across}$, is ~1/30 of G_{across} for single-layer graphene; it increases marginally when the thickness of graphene sheet increases but is still <10 MW/m^{2}K for three-layer graphenes. The large value of G_{across} is consistent with that reported in previous research [26,28]. The fact that $G_{non\text{-}across}$ is smaller than G_{across} for single-layer graphenes has been noted in Ref. [28]. However, the difference between $G_{non\text{-}across}$ and G_{across} in that work is much smaller than that observed here, probably due to the way that $G_{non\text{-}across}$ was extracted therein. Additionally, the mechanism behind the difference between G_{across} and $G_{non\text{-}across}$ (i.e., the duality of interfacial thermal conductance) was not discussed. Here we show that all of the above observations originate from the unique physical and chemical structure of single-layer and multi-layer graphenes.

Single-layer graphene has extraordinary chemical structure in the sense that adjacent carbon atoms form strong in-plane covalent sp^2 bonds whose bonding energy is even higher than the sp^3 bonds in diamonds [34]. Single-layer graphene also has an unusual physical structure in the sense that it is a single-atom thick, two-dimensional material. In single-layer graphene, the in-plane vibration is dominated by high frequency longitudinal (LA) and transverse (TA) modes [2], and its unique layer structure allows out-of-plane vibrations with both low and high frequency flexural (ZA) modes [2,25–27]. Multi-layer graphenes are stacks of single-layer graphenes, with neighboring layers bonded together through weak van der Waals forces. Because of the confinement by neighboring layers, the flexural mode of vibration in each graphene layer is considerably suppressed. Nevertheless, the coupling between the low-frequency out-of-plane vibrational modes of neighboring layers is a major channel for the thermal transport in the direction normal to the basal plane of graphene layers.

For the mode of interfacial thermal transport probed in Fig. 1a, energy enters graphene from one side of its basal plane mostly through the coupling between the low frequency vibrational mode of the liquid octane and the low frequency out-of-plane vibrational mode of the graphene, and leaves from the other side of graphene through the same channel. As clarified in prior studies [25,26,28], there is a very good overlap between the out-of-plane vibrational modes of graphene and the vibrational modes of liquid octane in the low frequency regime, and thus G_{across} is large. For the mode of interfacial thermal transport probed in Fig. 1b, the channel for energy transport is quite similar, i.e., the coupling between the vibrational mode of liquid octane and the out-of-plane vibrational mode of graphene plays an essential role in the energy transport. However, the energy transport in this second mode also demonstrates a two fold difference from that in the first mode. First, at any given lateral position, energy enters graphene *simultaneously through both sides* of the basal plane. Second, energy generally leaves graphene at a position on the basal plane that is far away from where it initially entered. The low $G_{non\text{-}across}$ observed for the second mode of interfacial thermal transport has two main origins.

First, the positive correlation of the heat transfer at the two sides of a graphene sheet, which originates from the thin thickness of graphene, reduces the effectiveness of thermal transport between the matrix (octane fluids) and the graphene sheet. To show this, we note that non-equilibrium thermal transport can be understood by studying the fluctuation of heat fluxes in equilibrium systems. Specifically, in an equilibrium system, the thermal conductance at the interface between two materials α and β is related to the fluctuation of instantaneous heat flux between them by a Green–Kubo type formula [35,36]

$$G^a_{equ} = \frac{1}{Ak_BT^2}\int_0^\infty \langle q_{\alpha\to\beta}(0)q_{\alpha\to\beta}(t)\rangle dt, \tag{5}$$

in which A is the surface area of the interface, k_B is the Boltzmann constant, and $q_{\alpha\to\beta}$ is the instantaneous heat flux from α to β given by

$$q_{\alpha\to\beta} = \sum_{i\in\alpha}\sum_{j\in\beta}\mathbf{F}_{ij}\cdot\mathbf{v}_j, \tag{6}$$

where $\mathbf{F}_{ij}$ is the force exerted by atom i in material α on atom j in material β, and $\mathbf{v}_j$ is the velocity of atom j. Although Eq. (5) is only exact when α and β are semi-infinite [36], it can be used to understand the interfacial thermal conductance qualitatively when one of the materials is finite in size. Using the system sketched in Fig. 1a but with heat injection/removal zones removed, we performed equilibrium molecular dynamics (EMD) simulations to compute the interfacial thermal conductance and the results are denoted as G^a_{equ}. In these simulations, each system is simulated for 500 ps in the NVE ensemble with 30 different initial configurations. Since each graphene sheet forms two interfaces with the fluids surrounding it, the area A in Eq. (5) is twice the project area of the graphene sheet A_{prj}. In calculating $q_{\alpha\to\beta}$ (α: graphene; β: liquid octane), we identify two contributions: $q_{\alpha\to\beta1}$and $q_{\alpha\to\beta2}$, which denote the heat flux from the graphene sheet to the liquid octane above and below it, respectively. Due to the symmetry between the liquid octane above and below graphene, $\langle q_{\alpha\to\beta1}(0)q_{\alpha\to\beta1}(t)\rangle = \langle q_{\alpha\to\beta2}(0)q_{\alpha\to\beta2}(t)\rangle$. This fact, along with $q_{\alpha\to\beta2} = -q_{\beta2\to\alpha}$, allows Eq. (5) to be reduced to

$$G^a_{equ} = G_1 - G_2 \tag{7a}$$

$$G_1 = \frac{1}{A_{prj}k_BT^2}\int_0^\infty \langle q_{\alpha\to\beta1}(0)q_{\alpha\to\beta1}(t)\rangle dt \tag{7b}$$

$$G_2 = \frac{1}{A_{prj}k_BT^2}\int_0^\infty \langle q_{\beta2\to\alpha}(0)q_{\alpha\to\beta1}(t)\rangle dt, \tag{7c}$$

where G_1 is the contribution of autocorrelation of the fluctuating heat flux at each graphene–octane interface and G_2 is the contribution of cross-correlation of fluctuating heat flux at the two opposing graphene–octane interfaces. Fig. 4a shows the running integration of the heat flux correlation functions for a single-layer graphene immersed in liquid octane. G_1 approaches 62.5 MW/m^{2}K at t = 50 ps, which indicates that the heat can be conducted from the graphene to the liquid octane above (or below) it relatively easily and vice versa. However, the fluctuating heat flux from the liquid octane below the graphene layer to the graphene layer is often positively correlated with the fluctuating heat flux from the graphene to the liquid octane above it (i.e., $\langle q_{\beta2\to\alpha}(0)q_{\alpha\to\beta1}(t)\rangle$ is predominantly positive at short time, cf. Fig. 4b) and thus G_2 is always positive. G_2 converges to ~48.4 MW/m^{2}K at t = 50 ps. Since, at large time, G_2 is close to G_1, it follows that G^a_{equ} is small, i.e., heat cannot be

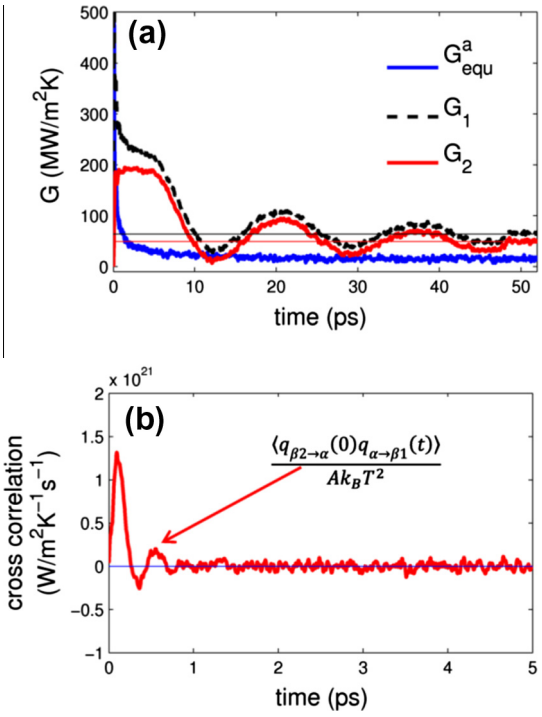

Fig. 4 – (a) Running integration of G^a_{equ}, G_1, G_2 given by Eqs. (7a)–(7c). (b) Cross-correlation function $\langle q_{\beta 2\to\alpha}(0)q_{\alpha\to\beta 1}(t)\rangle$ in Eq. (7c). The graphene sheet is a single-layer graphene. (A colour version of this figure can be viewed online.)

conducted easily from the graphene to the liquid octane above *and* below it simultaneously. The inefficient heat conduction from *all* the surrounding liquid octane to graphene, despite that the heat exchange between the graphene and either of the octane layers adjacent to it is effective, has a simple physical interpretation. Specifically, collisions between octane molecules above the graphene sheet with the graphene atoms allow heat to pass from these molecules to graphene. However, because the graphene layer is thin, following each such collision, the graphene atoms will likely collide with the octane molecules below them and thus pass heat to those molecules (this is evident from the fact that $\langle q_{\beta 2\to\alpha}(0)q_{\alpha\to\beta 1}(t)\rangle$ is predominantly positive at short time). Therefore, for an NEMD system as shown in Fig. 1b, the overall heat conduction from *all* surrounding liquid octane maintained at one temperature to a graphene sheet maintained at another temperature (quantified by G^a_{equ}), is not effective, and thus $G_{\text{non-across}}$ is small for thin graphene sheets. As the thickness of graphene sheet increases, the correlation between the molecular collisions at its two surfaces gradually disappears, and G_2 decreases toward zero. Consequently, G^a_{equ} increases with the graphene sheet thickness (see. Fig. 3), and this helps explain why $G_{\text{non-across}}$ increases when the number of layers in the graphene sheet increases.

The above analysis shows that we can gain insights into the physical origins of the small $G_{\text{non-across}}$ at small N_{gn} and its increase with N_{gn} by examining the fluctuation of interfacial heat fluxes in equilibrium systems. An interesting question is whether the large G_{across} can also be understood using similar methods, or more specifically, whether the large G_{across} can be obtained from appropriate Green–Kubo formula and EMD simulations. As shown in the Supplementary Information, for the interfacial thermal transport probed in Fig. 1a, in which the graphene sheet essentially serves as a *relay* for the heat transfer between the fluids at its two sides (i.e., heat enters the graphene from one side and then immediately leaves through the other side), the thermal conductance G_{across} can be computed using a new Green–Kubo formula. While such a Green–Kubo formula is rigorous only in the limit of hypothetical infinitely thin graphene sheets, it is quite accurate for single layer graphenes (see Supplementary Information).

The second mechanism that can cause the low $G_{\text{non-across}}$ in the systems shown in Fig. 1b is the large internal resistance due to the poor thermal coupling between the high frequency LA and TA modes and the low frequency ZA mode within the graphene sheet. In the system shown in Fig. 1b, heat enters/leaves the graphene sheet at different positions on its basal plane, but all are through the coupling between the low frequency out-of-plane vibrational mode of the graphene and the low frequency vibrational mode of the liquid octane. However, when graphene sheets are embedded inside matrix materials or supported on substrates, the flexural vibrational mode (ZA) with low frequency is damped [7]. Since the heat conduction in the in-plane direction has large contribution from the in-plane LA and TA phonon modes [6], which feature mostly high frequency components, the interfacial thermal resistance in systems in Fig. 1b will involve an internal resistance component coming from the thermal coupling between the in-plane LA and TA phonons and the out-of-plane ZA phonons. Since the coupling between the LA/TA phonon modes with ZA phonon modes is relatively weak for both supported- and vacuum-suspended graphenes [6,23,37], such an internal resistance can also be large for immersed graphenes. Consequently, $G_{\text{non-across}}$ is significantly reduced. Since such an internal resistance does not change greatly when the thickness of a graphene sheet increases, $G_{\text{non-across}}$ remains small as the graphene sheet thickness increases. We note that the internal resistance within graphene has been found to lead to a low conductance of graphene–polymer interfaces in systems similar to Fig. 1a when the heat sink/source are placed inside the graphene during NEMD simulations [25].

We note that the internal coupling and resistance between the low-frequency ZA modes and the high-frequency LA/TA modes should always exist regardless of the heat transfer mode, and they are essential for establishing the equilibrium and steady state of graphene. While they affect greatly the interfacial thermal transport in the systems shown in Fig. 1b, their effects on the *steady state* thermal transport in the system shown in Fig. 1a are small. Specifically, in such systems, heat enters graphene through the coupling between graphene's low-frequency ZA modes and octane's low-frequency vibrational modes. At steady state, all heat entering graphene from octane on one side leaves the graphene from the other side, again through the coupling between graphene's low-frequency ZA modes and the low-frequency vibrational modes of the octane on the other side. The in-plane heat conduction does not exist here and there is little exchange of energy between graphene's low-f ZA modes and high-f LA/TA modes given that the graphene is only one

or several atoms thick in the heat transfer direction. Consequently, the internal coupling between graphene's low-f ZA modes and high-f LA/TA modes plays little role in the overall thermal transport across the plane and does not manifest itself in the interfacial thermal resistance [25]. We note that, however, if the graphene is not at a steady state, then the coupling between the ZA and the LA/TA modes can impact thermal transport even in systems shown in Fig. 1a. Envision that the heat source and sink (colored by red and blue) are disabled in the system shown in Fig. 1a, and the system is at a uniform temperature at $t = 0$. At $t > 0$, heat is added continuously into the heat source zone but the heat sink remains disabled. Clearly, the graphene's temperature will rise with time. Here, heat enters graphene via the coupling between graphene's low-frequency ZA modes and octane's low-frequency vibrational modes. Some of this heat will be stored in the graphene, which involves the exchange of energy between the ZA modes and the LA/TA modes. Therefore, the internal coupling between these modes affects how the temperature of graphene rises and thus the effective interfacial thermal resistance. Such an interesting situation merits further investigations in the future.

The above two effects, i.e., the strong correlations between fluctuating heat fluxes at two sides of a graphene sheet and the poor coupling between graphene's low-frequency ZA modes and high-frequency LA/TA modes, contribute to the low $G_{\text{non-across}}$. One can question whether they are intrinsic effects and whether they are correlated. We believe both effects are intrinsic in the sense that they originate from the unique physical and chemical structure of thin graphene sheets. The first effect is perhaps less intrinsic because it is also directly influenced by how the matrix materials (e.g., octane liquids in our study) interact with the graphene sheet. There likely exist some correlations between these two effects. The poor coupling between the low-frequency ZA modes and high-frequency LA/TA modes to some degree may facilitate the positive correlation of the fluctuating heat fluxes at two sides of a graphene sheet. This is because, if the coupling between these modes were good, the heat flux entering into graphene at a certain time instant through the coupling between graphene's low-frequency ZA modes and octane's low-frequency vibrational modes would likely propagate within graphene rather than quickly leave the graphene (and thus would reduce the positive correlation between the fluctuating heat fluxes at two sides of a graphene sheet). However, to what extent these two effects are correlated and how their correlations depend on the thickness of graphene sheet and the nature of the matrix materials are not well understood at present. Understanding these correlations can lead to a deeper appreciation of the interfacial thermal transport involving graphene sheets (or more generally, two-dimensional materials), and merits further investigations in the future.

The fact that the conductance of graphene-matrix interfaces depends on the mode of interfacial thermal transport has not yet received attention in the research community. However, such dependence should have rich ramifications in many practical problems. For example, in nanocomposites, the prevailing mode of interfacial thermal transport is that shown in Fig. 1b. Hence, it is important to use $G_{\text{non-across}}$ rather than the much larger G_{across} when optimizing the design of graphene-based nanocomposites. This can potentially affect the design strategy significantly: if the interfacial conductance is large (e.g., >100 MW/m^{2}K), then the negative impact of interfacial thermal transport on the effective thermal conductivity of graphene-based composites is limited; otherwise, the design must be tailored to minimize its impact, e.g., by utilizing graphene sheets with large length-to-thickness ratios as suggested in prior research [28]. The difference between $G_{\text{non-across}}$ and G_{across} must also be taken into account when interfacial thermal conductance is used in models to deduce other thermal properties. For example, to determine the thermal conductivity of graphene sheets embedded in a matrix, one can perform two independent experiments. In the first experiment, one measures the temperature distribution of the surrounding matrix when an external heating is imposed at a position near the embedded graphene sheet [8]. In the second experiment, one measures the thermal conductance of interfaces formed by the same materials in another independent setup. By fitting the measured matrix temperature distribution in the first experiment to that predicted by FEM models using the interfacial thermal conductance measured in the second experiment, one can extract the thermal conductivity of the graphene sheet. In such a method, it is essential that the interfacial conductance measured in the second experiment has the same mode of interfacial thermal transport as that in the first example. Otherwise, systematic errors can be introduced into the extracted thermal conductivities of graphene sheets.

4. Conclusions

NEMD simulations were used to study the conductance of graphene–octane interfaces under two different modes of interfacial thermal transport. When heat enters graphene from one side of its basal plane and leaves through the opposite side, the interfacial conductance, G_{across}, is ~150 MW/m^{2}K for a single-layer graphene and decreases as the thickness (number of layers) of the graphene sheet increases. When heat enters graphene from both sides at one position and leaves the graphene at a position far away on its basal plane, the interfacial conductance, $G_{\text{non-across}}$, is ~5 MW/m^{2}K for single-layer graphene and increases moderately as the graphene sheet thickness increases. For thick graphene layers, G_{across} is reproduced using the conventional Green–Kubo type formula for interfacial thermal conductance. G_{across} for single-layer graphene can be computed quite accurately using a new Green–Kubo formula derived by assuming that graphene serves as a relay for heat conduction between liquid octane on its two sides. The duality of G_{across} and $G_{\text{non-across}}$ as well as their dependence on the graphene sheet thickness originates from the positive coupling of the heat transfer on the two sides of graphene layers embedded in a matrix and from the internal resistance arising from the poor thermal coupling between high-frequency in-plane vibrational modes and low frequency out-of-plane vibrational modes within graphene. The numerical difference between G_{across} and $G_{\text{non-across}}$ may depend on the specific models used for graphene and the type of matrix materials, but their qualitative difference should remain because such differences can

be traced ultimately to the unique physical and chemical structures of the graphene layers. The dependence of the thermal conductance of graphene–matrix interface on the mode of interfacial thermal transport must be taken into account in research such as experimental characterization of thermal conductivity of graphene and design of graphene-based thermal nanocomposites.

Acknowledgments

The authors thank the CCIT office at Clemson University for allocation of computing time. R.Q. thank Drs. Feng Wang (University of Arkansas), Dongshan Wei (Chinese Academy of Science), and Peng Yi (MIT) for help during the initial stage of this research. R.Q. and B.Y. acknowledge support from NSF (grant No. 1336778 and 1336590). R.Q. was partially supported by an appointment to the HERE program for faculty at the Oak Ridge National Laboratory (ORNL) administered by ORISE. The authors at ORNL acknowledge the support from the Center for Nanophase Materials Sciences, which is sponsored at ORNL by the Scientific User Facilities Division, Office of Basic Energy Sciences, U.S. Department of Energy.

Appendix A. Supplementary data

Supplementary data associated with this article can be found, in the online version, at http://dx.doi.org/10.1016/j.carbon.2014.03.050.

REFERENCES

[1] Song W-L, Veca LM, Anderson A, Cao M-S, Cao L, Sun Y-P. Light-weight nanocomposite materials with enhanced thermal transport properties. Nanotechnol Rev 2012;1:363–76.
[2] Pop E, Varshney V, Roy AK. Thermal properties of graphene: fundamentals and applications. MRS Bull 2012;37:1273–81.
[3] Shi L. Thermal and thermoelectric transport in nanostructures and low-dimensional systems. Nanoscale Microscale Thermophys Eng 2012;16:79–116.
[4] Balandin AA. Thermal properties of graphene and nanostructured carbon materials. Nat Mater 2011;10:569–81.
[5] Sadeghi MM, Pettes MT, Shi L. Thermal transport in graphene. Solid State Commun 2012;152:1321–30.
[6] Qiu B, Ruan X. Reduction of spectral phonon relaxation times from suspended to supported graphene. Appl Phys Lett 2012;100:193101.
[7] Ong Z-Y, Pop E. Effect of substrate modes on thermal transport in supported graphene. Phys Rev B 2011;84:75471.
[8] Jang W, Chen Z, Bao W, Lau CN, Dames C. Thickness-dependent thermal conductivity of encased graphene and ultrathin graphite. Nano Lett 2010;10:3909–13.
[9] Seol JH, Jo I, Moore AL, Lindsay L, Aitken ZH, Pettes MT, et al. Two-dimensional phonon transport in supported graphene. Science 2010;328:213–6.
[10] Shahil KMF, Balandin AA. Graphene-multilayer graphene nanocomposites as highly efficient thermal interface materials. Nano Lett 2012;12:861–7.
[11] Veca LM, Meziani MJ, Wang W, Wang X, Lu F, Zhang P, et al. Carbon nanosheets for polymeric nanocomposites with high thermal conductivity. Adv Mater 2009;21:2088–92.
[12] Liang Q, Yao X, Wang W, Liu Y, Wong CP. A three-dimensional vertically aligned functionalized multilayer graphene architecture: an approach for graphene-based thermal interfacial materials. ACS Nano 2011;5:2392–401.
[13] Sun X, Ramesh P, Itkis ME, Bekyarova E, Haddon RC. Dependence of the thermal conductivity of two-dimensional graphite nanoplatelet-based composites on the nanoparticle size distribution. J Phys Condens Matter 2010;22:334216.
[14] Nan C-W, Birringer R, Clarke DR, Gleiter H. Effective thermal conductivity of particulate composites with interfacial thermal resistance. J Appl Phys 1997;81:6692.
[15] Gao JW, Zheng RT, Ohtani H, Zhu DS, Chen G. Experimental investigation of heat conduction mechanisms in nanofluids. Clue on clustering. Nano Lett 2009;9:4128–32.
[16] Wu C, Cho TJ, Xu J, Lee D, Yang B, Zachariah MR. Effect of nanoparticle clustering on the effective thermal conductivity of concentrated silica colloids. Phys Rev E 2010;81:11406.
[17] Wang JJ, Zheng RT, Gao JW, Chen G. Heat conduction mechanisms in nanofluids and suspensions. Nano Today 2012;7:124–36.
[18] Yang B, Han ZH. Thermal conductivity enhancement in water-in-FC72 nanoemulsion fluids. Appl Phys Lett 2006;88:261914.
[19] Yang J, Yang Y, Waltermire SW, Gutu T, Zinn AA, Xu TT, et al. Measurement of the intrinsic thermal conductivity of a multiwalled carbon nanotube and its contact thermal resistance with the substrate. Small 2011;7:2334–40.
[20] Yang J, Waltermire S, Chen Y, Zinn AA, Xu TT, Li D. Contact thermal resistance between individual multiwall carbon nanotubes. Appl Phys Lett 2010;96:023109.
[21] Merabia S, Termentzidis K. Thermal conductance at the interface between crystals using equilibrium and nonequilibrium molecular dynamics. Phys Rev B 2012;86:94303.
[22] Alam H, Ramakrishna S. A review on the enhancement of figure of merit from bulk to nano-thermoelectric materials. Nano Energy 2013;2:190–212.
[23] Zhang J, Huang X, Yue Y, Wang J, Wang X. Dynamic response of graphene to thermal impulse. Phys Rev B 2011;84:235416.
[24] Zhang C, Zhao W, Bi K, Ma J, Wang J, Ni Z, et al. Heat conduction across metal and nonmetal interface containing imbedded graphene layers. Carbon 2013;64:61–6.
[25] Hu L, Desai T, Keblinski P. Determination of interfacial thermal resistance at the nanoscale. Phys Rev B 2011;83:195423.
[26] Luo T, Lloyd JR. Enhancement of thermal energy transport across graphene/graphite and polymer interfaces: a molecular dynamics study. Adv Funct Mater 2012;22:2495–502.
[27] Konatham D, Papavassiliou DV, Striolo A. Thermal boundary resistance at the graphene–graphene interface estimated by molecular dynamics simulations. Chem Phys Lett 2012;527:47–50.
[28] Hu L, Desai T, Keblinski P. Thermal transport in graphene-based nanocomposite. J Appl Phys 2011;110:033517.
[29] Liu J, Alhashme M, Yang R. Thermal transport across carbon nanotubes connected by molecular linkers. Carbon 2012;50:1063–70.
[30] Kim BH, Beskok A, Cagin T. Molecular dynamics simulations of thermal resistance at the liquid–solid interface. J Chem Phys 2008;129:174701.
[31] Maiti A, Mahan GD, Pantelides ST. Dynamical simulations of nonequilibrium processes – heat flow and the Kapitza resistance across grain boundaries. Solid State Commun 1997;102:517–21.
[32] Wei D, Song Y, Wang F. A simple molecular mechanics potential for μm scale graphene simulations from the

adaptive force matching method. J Chem Phys 2011;134:184704.
[33] Yi P, Rutledge GC. Molecular simulation of bundle-like crystal nucleation from n-eicosane melts. J Chem Phys 2011;135:24903.
[34] Katsnelson MI. Graphene: carbon in two dimensions. Mater. Today 2007;10:20–7.
[35] Puech L, Bonfait G, Castaing B. Mobility of the3He solid-liquid interface. Experiment and theory. J Low Temp Phys 1986;62:315–27.
[36] Barrat J-L, Chiaruttini F. Kapitza resistance at the liquid–solid interface. Mol Phys 2003;101:1605–10.
[37] Zhang H, Lee G, Cho K. Thermal transport in graphene and effects of vacancy defects. Phys Rev B 2011;84:115460.